

Magnetic and non-Fermi-liquid properties of $U_{1-x}La_xPd_2Al_3$

V. S. Zapf, R. P. Dickey, E. J. Freeman, C. Sirvent, and M. B. Maple

Department of Physics and Institute for Pure and Applied Physical Sciences, University of California, San Diego, La Jolla, California 92093

(Received 25 May 2001; published 19 December 2001)

We have performed measurements of the temperature dependence of the electrical resistivity, specific heat, and magnetic susceptibility of polycrystalline samples of $U_{1-x}La_xPd_2Al_3$. The antiferromagnetic order of the parent compound UPd_2Al_3 is rapidly suppressed for small lanthanum concentrations $0 \leq x \leq 0.2$. For samples with lanthanum concentrations $0.25 \leq x \leq 0.65$, magnetic relaxation and ac magnetic-susceptibility measurements indicate the formation of a spin-glass state with a freezing temperature that extrapolates to $T=0$ K near $x=0.8$. Non-Fermi-liquid temperature dependences in the electrical resistivity $\rho(T)$ and specific heat $C(T)$ were observed for samples with $x=0.8$ and 0.9 . The resistivity $\rho(T)$ at low temperatures can be described by a power law $\rho/\rho_0 = 1 - AT^n$ for $T < 10$ K with $n = 1.3 \pm 0.1$ for the samples with $x=0.8$ and 0.9 . The electronic specific-heat coefficient $\Delta C/T$ has a logarithmic temperature dependence in the temperature ranges $3 \text{ K} \leq T \leq 20 \text{ K}$ ($x=0.8$) and $1 \text{ K} \leq T \leq 6 \text{ K}$ ($x=0.9$).

DOI: 10.1103/PhysRevB.65.024437

PACS number(s): 75.20.Hr, 71.27.+a, 71.10.Hf, 75.50.Lk

I. INTRODUCTION

The subject of non-Fermi-liquid (NFL) behavior in f -electron systems has attracted an increasing amount of attention in recent years. NFL behavior has been observed in a number of Ce-, Yb-, and U-based heavy-fermion intermetallic compounds. In certain stoichiometric compounds, e.g., $CeNi_2Ge_2$ and $YbRh_2Si_2$, the NFL behavior appears at zero pressure,¹⁻³ whereas in other compounds, e.g., $CeIn_3$ and $CePd_2Si_2$, NFL behavior appears with the application of hydrostatic pressure.^{4,5} NFL behavior is also seen in a growing class of compounds in which the magnetic ion (Ce, Yb, or U) is diluted with a nonmagnetic rare earth or actinide, e.g., $U_{1-x}Th_xPd_2Al_3$ and $Y_{1-x}U_xPd_3$.⁶ In some cases, substitution at a ligand site also results in NFL behavior, as is the case with $UCu_{5-x}M_x$ ($M = Pd, Pt$),^{7,8} The NFL behavior is manifested as power law or logarithmic divergences of physical properties at low temperatures, notably the electrical resistivity $\rho(T)$, specific heat $C(T)$, and magnetic susceptibility $\chi(T)$. These properties typically show the following temperature dependences: (i) $\rho(T) \sim 1 - a(T/T_0)^n$, where $|a| \sim 1$, $a < 0$ or > 0 , and $n \sim 1 - 1.5$; (ii) $C(T)/T \sim (-1/T_0) \ln(T/T_0)$, or $\sim T^{-1+\lambda}$; and (iii) $\chi(T) \sim 1 - (T/T_0)^{1/2}$, $\sim (-1/T_0) \ln(T/T_0)$, or $\sim T^{-1+\lambda}$ ($\lambda \sim 0.7 - 0.8$). In several systems, the characteristic temperature T_0 can be identified with the Kondo temperature T_K .

Several theories have been advanced to explain NFL behavior in f -electron materials. One scenario involves isolated impurities that lead to a two-channel spin-1/2 Kondo effect.⁹⁻¹² Another picture assumes a cooperative effect associated with a second-order magnetic phase transition that has been suppressed to $T=0$ K by chemical substitution, hydrostatic pressure, or magnetic fields.¹³⁻¹⁶ The discovery of several materials that have a spin-glass transition, as opposed to a magnetic phase transition, suppressed to $T=0$ K, has prompted the development of theories describing NFL behavior in the vicinity of a spin-glass freezing temperature that has been suppressed to $T=0$ K.^{17,18} A distribution of

Kondo temperatures due to atomic disorder has also been proposed to account for NFL behavior in the alloyed compounds.¹⁹ Finally, the Griffith's phase model assumes a combination of disorder and competition between the Ruderman-Kittel-Kasuya-Yosida (RKKY) and the Kondo interactions in alloyed compounds.²⁰ Despite a wealth of theories, most f -electron system that exhibit NFL behavior remain largely unexplained. Thus, these materials continues to pose an interesting puzzle.

Recently the heavy-fermion superconductor UPd_2Al_3 has been shown to exhibit NFL behavior when uranium is partially replaced by thorium^{21,22} or yttrium.²³ The parent compound UPd_2Al_3 orders antiferromagnetically (AFM) below the Néel temperature $T_N = 14.6$ K and exhibits superconductivity that coexists with magnetic order below $T_c = 2$ K.²⁴ Chemical substitution with thorium or yttrium in place of uranium results in a suppression of the magnetic order and the superconductivity, but the nature of this suppression and the resulting phase diagrams are remarkably different in $U_{1-x}Th_xPd_2Al_3$ and $U_{1-x}Y_xPd_2Al_3$. Substituting thorium onto the uranium site causes a very gradual suppression of T_N and T_c , while the features in the magnetic susceptibility and specific heat associated with AFM order and the superconducting transition are suppressed rapidly with increasing thorium concentration. Both AFM and superconductivity vanish in a crossover region between $x=0.2$ and 0.4 and NFL behavior is observed for concentrations in the range $0.6 \leq x \leq 0.99$. In contrast, substituting with yttrium sharply suppresses both T_N and T_c . Superconductivity is suppressed below the low temperature limit of the experiments at $x=0.02$ and long-range magnetic order vanishes near $x=0.3$ and is replaced by a region of spin-glass behavior between $x=0.3$ and 0.7 .^{25,28} The spin-glass freezing temperature T_{SG} extrapolates to $T=0$ K at $x=0.7$, and NFL behavior is observed for $0.7 \leq x \leq 0.8$.²³ A recent study has suggested that the NFL behavior seen in $U_{1-x}Th_xPd_2Al_3$ can be associated with a single-ion effect, whereas the NFL behavior in the $U_{1-x}Y_xPd_2Al_3$ compound results from quantum

critical effects near a $T=0$ K quantum critical point.²⁹ The striking difference in behavior between the $U_{1-x}Y_xPd_2Al_3$ and $U_{1-x}Th_xPd_2Al_3$ systems raises the question of what aspect of the substituent element drives the NFL behavior. Is the lattice expansion due to the larger size of the thorium atom important, or is the valence of the substituent element significant? Thorium is tetravalent, whereas yttrium is trivalent in these compounds. In this paper, we investigate a third system, $U_{1-x}La_xPd_2Al_3$, in which trivalent lanthanum has been substituted for uranium. Comparison of the behavior of this system with that of $U_{1-x}Y_xPd_2Al_3$ and $U_{1-x}Th_xPd_2Al_3$ could shed some light on the role of the substituent species in driving the NFL behavior. Preliminary studies of the $U_{1-x}La_xPd_2Al_3$ system show^{25,30} the suppression of the Néel temperature for increasing lanthanum concentration x . In this paper, we expand on these studies. Based on measurements of electronic specific heat, magnetic susceptibility, and electrical resistivity, we present the phase diagram of this system and investigate NFL behavior therein.

II. EXPERIMENTAL DETAILS

The polycrystalline samples of $U_{1-x}La_xPd_2Al_3$ were prepared by arc-melting the constituent elements (U: 3N; La: 4N; Pd: 4N; Al: 5N) in stoichiometric amounts on a copper hearth in an ultra-high-purity argon atmosphere. The arc-melted ingots were then wrapped in tantalum foil and annealed in an argon atmosphere for seven days at 900 °C. X-ray-powder-diffraction measurements showed that all samples consist of a single phase with the hexagonal $PrNi_2Al_3$ structure. Lattice constants were determined from a linear regression analysis of the x-ray-diffraction peaks. For comparison, lattice constants of samples of $U_{1-x}Y_xPd_2Al_3$ and $U_{1-x}Th_xPd_2Al_3$ were also determined.

The magnetization M was measured as a function of time t , magnetic field H , and temperature T using two commercial superconducting quantum interference device (SQUID) magnetometers (Quantum Design) with maximum fields of 5.5 and 7 T. The dc magnetic susceptibility $\chi_{dc}(T)$ was determined from the initial slope of the $M(H)$ curves between 0 and 100 Oe. In-phase ac magnetic susceptibility $\chi_{ac}(T)$ of the samples with $0.1 \leq x \leq 0.65$ was measured using a commercial SQUID magnetometer at frequencies in the range $1 \text{ Hz} \leq f \leq 1000 \text{ Hz}$ with an amplitude of 1 Oe. For the samples with $x=0.7$ and 0.8 , $\chi_{ac}(T)$ was measured in a ^3He - ^4He dilution refrigerator down to $T=100$ mK ($x=0.7$) and $T=55$ mK ($x=0.8$) in an applied field of 0.05 Oe at 12 Hz.

The electrical resistivity $\rho(T)$ was measured using a standard four-wire technique at temperatures in the range $1.2 \text{ K} \leq T \leq 300 \text{ K}$ in a ^4He cryostat with an applied ac current of 1 mA at 16 Hz. Gold pads were deposited on the samples with a sputtering system (Hummer 6.2) and gold wires were attached with a two-part silver epoxy (Epotek H20E). Measurements of $\rho(T)$ at low temperatures were performed in a ^3He - ^4He dilution refrigerator at temperatures down to 60 mK using a linear research LR-700 bridge with an applied ac current of 100 μA at 12 Hz. The specific heat was measured using a semiadiabatic technique in a ^3He cryostat for 0.5 K

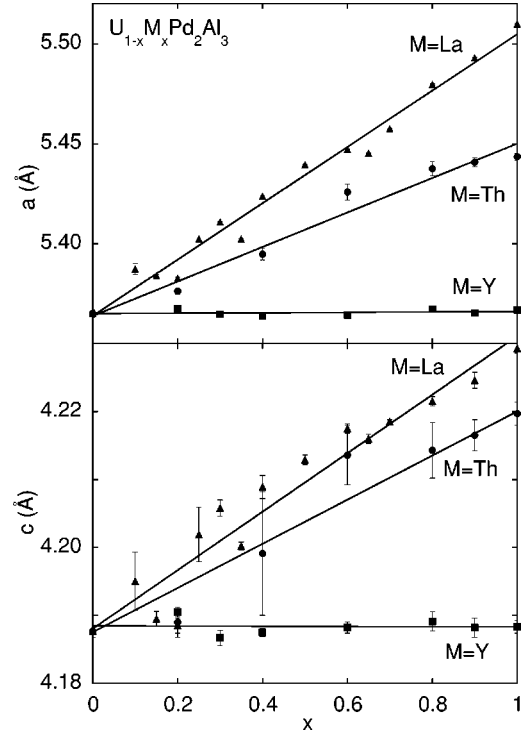


FIG. 1. Hexagonal lattice parameters a (upper figure) and c (lower figure) as a function of substituent concentration x for the $U_{1-x}La_xPd_2Al_3$, $U_{1-x}Th_xPd_2Al_3$, and $U_{1-x}Y_xPd_2Al_3$ systems. The straight lines are linear fits to the data.

$\leq T \leq 120$ K.

III. RESULTS

The hexagonal lattice constants a and c determined from x-ray diffraction measurements are displayed in Fig. 1. The results show that substitution of lanthanum or thorium expands the lattice of the parent compound UPd_2Al_3 , whereas substitution of yttrium does not affect the lattice constants to within experimental error. The lines shown in Fig. 1 are linear fits of the lattice constants as a function of substituent concentration x .

The inverse dc magnetic susceptibility (χ_{dc}^{-1}) is plotted as a function of temperature T for $0 \text{ K} < T \leq 300 \text{ K}$ in Fig. 2(a) for the samples with $0.15 \leq x \leq 0.8$. The $\chi_{dc}^{-1}(T)$ data of all of the samples show significant curvature in the measured temperature range, and thus cannot be fit by a Curie-Weiss law. However, if a constant offset χ_0 is subtracted from each data set, a Curie-Weiss law of the form $\chi_{dc}(T) - \chi_0 = N\mu_{\text{eff}}^2/3k_B(T - \theta_{\text{CW}})$ can be fit to the magnetic-susceptibility data of the samples with $0.2 \leq x \leq 0.8$. The constant χ_0 is chosen such that $[\chi(T) - \chi_0]^{-1}$ is linear in T for $50 \text{ K} \leq T \leq 300 \text{ K}$. The values of χ_0 , which range from $2.4 \times 10^{-4} \text{ cm}^3/\text{mol}$ to $6.5 \times 10^{-4} \text{ cm}^3/\text{mol}$, are large compared to the Pauli susceptibility $\chi_P \sim 4.6 \times 10^{-5} \text{ cm}^3/\text{mol}$. This value of χ_P is an upper limit that is estimated from the relation $\chi_P/\gamma(\pi^2k_B^2/3\mu_B^2) \sim 1$, where a value of $\gamma = C/T = 150 \text{ mJ/mol K}$ for the compound UPd_2Al_3 is used.²⁴ Thus, it is likely that the curvature in χ_{dc}^{-1} is due to other effects than the Pauli susceptibility, such as a Van-Vleck contribution to the magnetic susceptibility, or crystal-field splitting of the U-ion $5f$ levels. The values of χ_0 , θ_{CW} , and μ_{eff} deter-

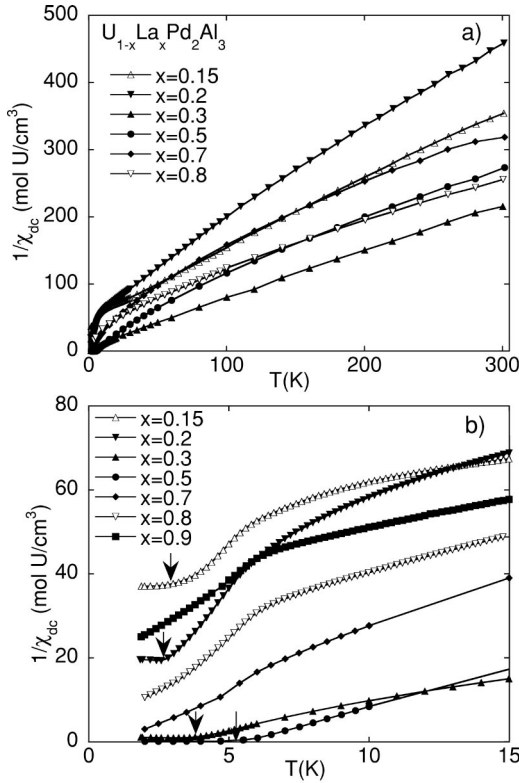


FIG. 2. (a) Inverse dc magnetic susceptibility χ_{dc}^{-1} of various $U_{1-x}La_xPd_2Al_3$ compounds as a function of temperature T , measured in an applied field of 1 kOe. The lines are guides to the eye. (b) Expanded view of the data below $T=15$ K in which the arrows indicate magnetic-ordering temperatures.

mined from the Curie-Weiss fits are listed in Table I. The Curie-Weiss temperatures θ_{CW} range from -1 to -88 K and the effective moments μ_{eff} range from $3.8\mu_B/U$ for the UPd_2Al_3 end member to $2.2\mu_B/U$ for $U_{1-x}La_xPd_2Al_3$ with $x=0.9$. The effective moments for the samples containing lanthanum are reduced from the free uranium ion moment of $3.56\mu_B$. The scatter in the values of μ_{eff} and θ_{CW} could be an artifact due to crystalline electric fields, as well as the fact that the measurements were performed on polycrystals, whereas measurements of the magnetic susceptibility of single crystals reveal a strong anisotropy between the magnetization along the c axis and in the $a-b$ plane.²⁶

In Fig. 2(b) the inverse magnetic susceptibility χ_{dc}^{-1} is shown for temperatures in the range $0 \text{ K} < T \leq 15 \text{ K}$. The χ_{dc}^{-1} vs T curves of all of the compounds exhibit a broad change in slope between 5 and 8 K. The arrows identify the location of features in χ_{dc} that roughly correspond to peaks seen in $\chi_{ac}(T)$ (see Fig. 12).

Measurements of ac magnetic susceptibility $\chi_{ac}(T)$ were made as a function of T for samples with $0.1 \leq x \leq 0.8$. The $\chi_{ac}(T)$ curves for the samples with $0.1 \leq x \leq 0.2$ show an abrupt change in slope, as seen in Fig. 3(a), which is typical of an antiferromagnetic phase transition. The Néel temperature T_N decreases from 14.6 K for the host compound UPd_2Al_3 to 2.7 K for the sample with $x=0.2$. The compounds with $0.25 \leq x \leq 0.35$ show a sharp peak in $\chi_{ac}(T)$. For clarity, these peaks have been plotted on a logarithmic scale

TABLE I. Curie-Weiss parameters μ_{eff} , θ_{CW} , and χ_0 , and magnetic transition temperatures T_N and T_{SG} for samples of $U_{1-x}La_xPd_2Al_3$ with $0 \leq x \leq 0.9$. The temperature-independent magnetic susceptibility χ_0 was chosen to linearize $[\chi(T) - \chi_0]^{-1}$ for $50 \leq T \leq 300$ K. The Curie-Weiss temperature θ_{CW} and effective moment per uranium atom μ_{eff} were determined from fits of $\chi(T) - \chi_0 = N_A \mu_{eff}^2 / 3k(T - \theta_{CW})$ to the $\chi_{dc}(T)$ data. The Néel temperatures T_N and spin-glass freezing temperatures T_{SG} were determined from peaks in the ac magnetic susceptibility.

x	$\mu_{eff}(\mu_B)$	θ_{CW} (K)	$10^{-4}\chi_0$ (cm ³ /mol)	T_N (K)	T_{SG} (K)
0	3.77 ^a	-52 ^a	-4.0 ^a	14.6	
0.10	3.2	-28	2.7	9.2	
0.15	2.5	-81	3.6	4.3	
0.20	2.2	-27	3.2	2.8	
0.25	2.6	-13	6.5		3.0
0.30	3.1	-1	3.5		3.4
0.35	2.7	-13	6.5		3.8
0.40	2.7	-8	4.8		4.9
0.50	2.6	-8	4.0		4.9
0.60	2.5	-15	4.0		3.6
0.65	2.6	-4	2.8		2.1
0.70	2.2	-19	3.6		1.4
0.80	2.7	-30	2.4		
0.90	2.2	-88	10		

^a $H = 5$ kOe.

in Fig. 3(b). The temperature of the maximum in χ_{ac} , T_{peak} , increases linearly with lanthanum concentration, as shown in the top inset. The bottom inset of Fig. 3(b) shows the magnitude of χ_{ac} at the peak temperature as a function of x , which also increases with the lanthanum concentration.

Figure 4 shows $\chi_{ac}(T)$ data for samples with $0.4 \leq x \leq 0.7$. The samples with $0.4 \leq x \leq 0.6$ have a double-peak feature in $\chi_{ac}(T)$, whereas the samples with $x=0.65$ and 0.7 (inset) have only one peak in the measured temperature range. For the sample with $x=0.8$, $\chi_{ac}(T)$ measured at temperatures down to $T=50$ mK showed no peaks or other features. There is no correlation between either T_{peak} or the magnitude of $\chi_{ac}(T)$ at T_{peak} with lanthanum concentration for the samples with $0.4 \leq x \leq 0.7$. The temperatures of these peaks in $\chi_{ac}(T)$ are indicated in the phase diagram in Fig. 12.

Disorder due to the presence of magnetic uranium and nonmagnetic lanthanum on the same lattice site could lead to the formation of a magnetic spin-glass state at low temperatures. In order to distinguish between spin-glass freezing and long-range order, we measured the relaxation of the dc magnetization M as a function of time t . The samples were cooled in zero field to $T=2$ K, a magnetic field of 10 Oe was applied, and the magnetization was measured as a function of time for 90 min. In Fig. 5, the magnetization M is plotted as a function of time t on a logarithmic scale for $0 \leq t \leq 90$ min. The magnetization of the samples in the range $0.25 \leq x \leq 0.65$ increases with a logarithmic time dependence, which is typical for spin or cluster glasses, in which multiple relaxation time constants are present.³¹ The samples with $x=0.15$ and 0.2 show no relaxation over the course of 90 min.

We investigated the spin-glass behavior further by means

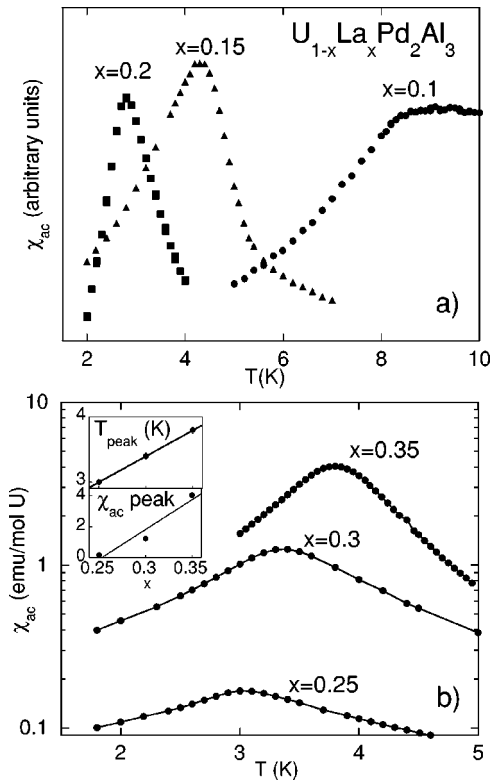


FIG. 3. (a) ac magnetic susceptibility χ_{ac} at 100 Hz as a function of temperature T for the compounds with $0.1 \leq x \leq 0.2$. The data have been scaled to fit on one plot. (b) ac magnetic susceptibility χ_{ac} at 100 Hz as a function of temperature T for the compounds with $0.25 \leq x \leq 0.35$. χ_{ac} is plotted on a log scale for clarity. The top inset shows the temperatures of the peaks T_{peak} in χ_{ac} as a function of lanthanum concentration x . The bottom inset shows the magnitude of χ_{ac} at T_{peak} as a function of x . The lines in the insets are linear fits to the data.

of ac magnetic-susceptibility $\chi_{ac}(T)$ measurements at different frequencies. For the samples with $x=0.2, 0.35$, and 0.6 , $\chi_{ac}(T)$ was measured in applied ac magnetic fields at frequencies of 1 Hz, 100 Hz, and 1000 Hz. These data are plotted in Fig. 6. The temperature of the peak in $\chi_{ac}(T)$,

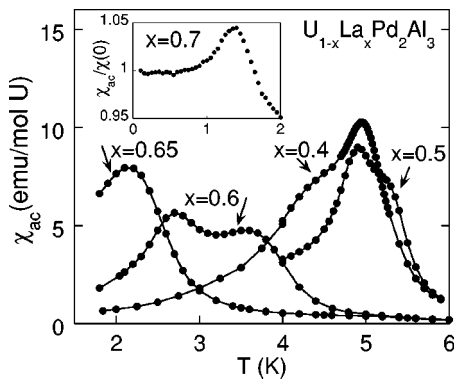


FIG. 4. ac magnetic susceptibility χ_{ac} in units of emu/mol U at 100 Hz as a function of temperature T for the compounds with $0.4 \leq x \leq 0.65$. The inset shows $\chi_{ac}(T)/\chi_{ac}(0)$ at 16 Hz for the sample with $x=0.7$.

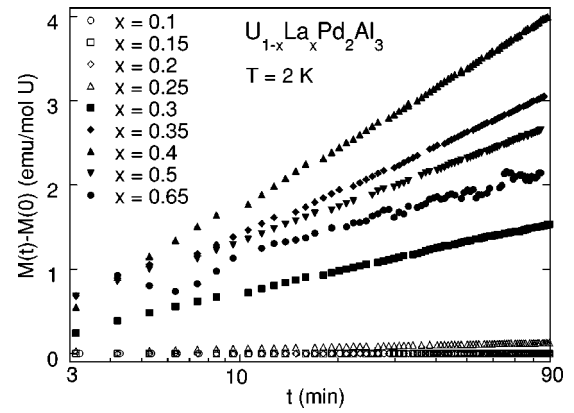


FIG. 5. dc magnetization $M(t) - M(0)$ as a function of time t in minutes for samples with $0.1 \leq x \leq 0.65$ at $T = 2$ K on a logarithmic scale.

T_{peak} shows no frequency dependence for the sample with $x=0.2$. By contrast, T_{peak} for the sample with $x=0.35$ increases slightly with frequency at a rate of 0.05 K/decade. $\chi_{ac}(T)$ of the sample with $x=0.6$ shows two peaks, both of which shift slightly with frequency. Therefore, we can conclude that the samples with $x=0.35$ and 0.6 exhibit spin-

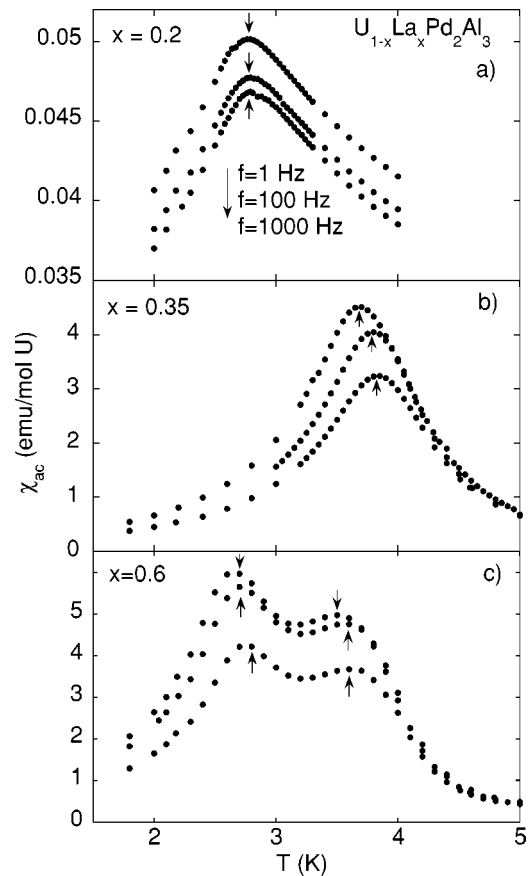


FIG. 6. ac magnetic susceptibility χ_{ac} as a function of temperature T at frequencies of 1 Hz (top curve), 100 Hz (middle curve), and 1 kHz (bottom curve) for the sample with $x=0.2$ (a), $x=0.35$ (b) and $x=0.6$ (c). The arrows indicate the peak value of χ_{ac} at each frequency.

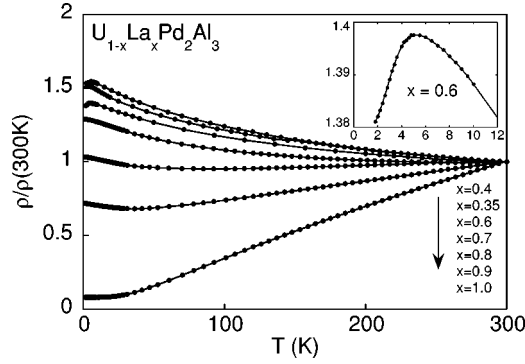


FIG. 7. Electrical resistivity $\rho(T)$ normalized to its value at $T=300$ K as a function of temperature T . The curves, in descending order, are for the samples with $x=0.4, 0.35, 0.6, 0.7, 0.8, 0.9$, and 1.0 . The inset shows $\rho(T)$ at low temperatures for the sample with $x=0.6$.

glass freezing, whereas the sample with $x=0.2$, which shows no frequency dependence of T_{peak} , exhibits long-range magnetic order.

Figure 7 shows the electrical resistivity $\rho(T)$ for samples in the range $0.35 \leq x \leq 1.0$. The superconducting transition of filamentary aluminum at $T_c=1.2$ K has been suppressed with an applied magnetic field of 300 Oe. The resistivities of the compounds $x=0.8$ and 0.9 are metallic in nature ($d\rho/dT > 0$) at high temperatures but show an increase with decreasing temperature, indicative of a Kondo effect at low temperatures. For the compounds with $0.35 \leq x \leq 0.7$, the Kondo scattering is so strong that $d\rho/dT < 0$ up to $T=300$ K. The samples with $x < 0.7$ show broad peaks in the $\rho(T)$ data at low temperatures, displayed for the sample with $x=0.6$ in the inset. The temperature at which these peaks occur is slightly higher than the temperature of the peaks in $\chi_{\text{ac}}(T)$, as can be seen in the phase diagram in Fig. 12. Broad peaks in the electrical resistivity have been observed in other spin glasses, such as $U_{1-x}Y_xPd_2Al_3$ and $Y_{1-x}U_xPd_3$, although not necessarily near the spin-glass freezing temperature.^{27,28}

The Kondo temperature T_K can be determined from the high-temperature $\rho(T)$ data for the samples with $x=0.8$ and 0.9 . The resistivity can be written as $\rho(T) = \rho_K(T) + \rho_L(T) + \rho_c$, where $\rho_K(T)$ is a Kondo scattering term, $\rho_L(T)$ is the lattice contribution to the resistivity, and ρ_c is a temperature-independent term due to potential scattering. The Kondo term $\rho_K(T)$ decreases with the logarithm of T for $T > T_K$ until it saturates at high temperatures, whereas the lattice term $\rho_L(T)$ typically increases linearly with T for temperatures on the order of 300 K. For the samples with $x=0.8$ and 0.9 , the resistivity $\rho(T)$ of the pure $LaPd_2Al_3$ sample has been subtracted in order to remove lattice contributions. Since $LaPd_2Al_3$ contains no magnetic ions, its resistivity is dominated by lattice contributions, and since the lattice constants of the samples with $x=0.8, 0.9$, and 1.0 are very similar, it is reasonable to assume that they all have similar lattice contributions to $\rho(T)$. Due to the porosity of the samples, and uncertainties in the geometrical factors, the exact resistivities are difficult to determine. Therefore, to accurately subtract the lattice contribution from the measured resistivities, we scaled the slopes of the

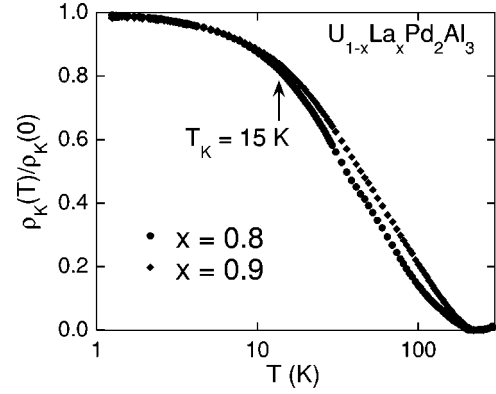


FIG. 8. Kondo contribution to the electrical resistivity $\rho_K(T)$, normalized to its extrapolated value at $T=0$ K, as a function of temperature T on a log scale for $x=0.8$ and 0.9 . The Kondo temperature T_K is taken as the point where $\rho_K(T)$ reaches 80% of its maximum value.

high-temperature linear regions of $\rho(T)$ to the slope of $\rho(T)$ of $LaPd_2Al_3$. The constant term ρ_c was chosen such that $\rho_K(T)$ saturates to zero at high temperatures, as is expected for Kondo scattering far above T_K .

In Fig. 8, $\rho_K(T)/\rho_K(0)$ is plotted as a function of temperature on a log scale for the samples with $x=0.8$ and 0.9 . As is expected for Kondo scattering, $\rho_K(T)$ increases logarithmically with decreasing temperature for $20 \text{ K} \leq T \leq 100 \text{ K}$. The Kondo temperature was approximated to be the temperature at which $\rho_K(T)$ reaches 80% of its maximum value, which is roughly the temperature at which $\rho_K(T)$ deviates from logarithmic behavior. This procedure yields Kondo temperatures of $T_K=15$ and 17 K for the samples with $x=0.8$ and 0.9 , respectively.

The low-temperature resistivity data for the samples with $x=0.8$ and 0.9 can be described by a power law of the form $\rho_K(T)/\rho_0 = 1 - AT^n$, where ρ_0 , A , and n are adjustable fitting parameters. We looked for a fit that describes the data at the lowest temperatures, and extends over the largest possible temperature range. Figure 9 shows the $\rho_K(T)$ data and the power-law fits (solid lines) for the samples with $x=0.8$ and $x=0.9$. Shown in the insets to Fig. 9, are plots of $1 - \rho_K(T)/\rho_0$ as a function of T on a log-log scale. In these plots, the power-law fits are straight lines. For the sample with $x=0.9$, we found that a power law with $n=1.3 \pm 0.1$, $A=5.3 \text{ mK}^{1/1.3}$, and $\rho_0=48 \mu\Omega \text{ cm}$ fits well for $65 \text{ mK} \leq T \leq 9 \text{ K}$. The $\rho(T)$ data for the sample with $x=0.8$ has a small peak at $T=0.5$ K, and a slight upturn at the lowest temperatures. It is possible that the peak is associated with a spin-glass transition at lower temperatures; therefore, it has been excluded from the power-law fit. Above $T=0.8$ K, the $\rho_K(T)$ data can be fit by a power law with $n=1.3 \pm 0.1$, $A=65 \text{ mK}^{1/1.3}$, and $\rho_0=72 \mu\Omega \text{ cm}$ up to $T=10$ K. The power-law fits are insensitive to the details of the subtraction of the phonon contributions, since those are much smaller than the electronic contributions at $T < 10$ K. The power law with $n=1.3$ for the $x=0.8$ and 0.9 samples is clearly at variance with Landau's Fermi-liquid theory, which predicts a power law T dependence with a $n=2$ exponent.

Figure 10 shows the specific heat divided by temperature $\Delta C(T)/T = C(x,T)/T - C(1,T)/T$ plotted as a function T on a log scale for the samples with $x=0.8$ and 0.9 . The specific

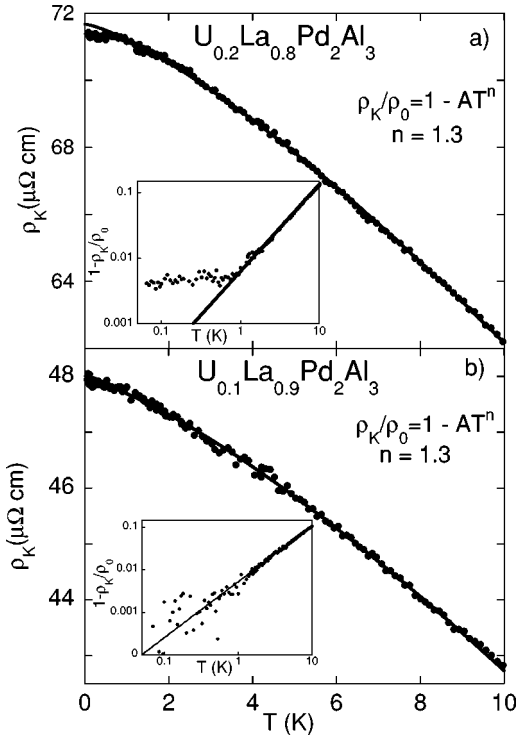


FIG. 9. Resistivity ρ_K as a function of temperature T for the sample with $x=0.8$ (a) and $x=0.9$ (b). The lines are fits of a power law $\rho_K(T)/\rho_0 = 1 - AT^n$ to the $\rho_K(T)$ data, where ρ_0 , A and n are fitting parameters. The inset shows $1 - \rho_K(T)/\rho_0$ vs T on a log-log scale, in which the power-law fitting function is a straight line.

heat of LaPd_2Al_3 , $C(1, T)$ has been subtracted from the specific heat of the other samples $C(x, T)$ to remove the phonon contributions. Since LaPd_2Al_3 displays a superconducting transition at $T \sim 0.8$ K, its normal-state specific heat was extrapolated to the lowest temperatures for the purpose of subtracting it from the data of other samples. In a Fermi liquid, $\Delta C(T)/T$ approaches a constant value at the lowest temperatures, whereas for the samples with $x=0.8$ and 0.9 , $\Delta C(T)/T$ clearly increases at the lowest temperatures. The solid lines in Fig. 10 are fits of the form $\Delta C(T)/T = -B \ln(T/T_0)$ to the data. For the sample with $x=0.8$, the fit yields $B=22.7$ mJ/mol K² and $T_0=4.1$ K for temperatures in the range $3 \text{ K} \leq T \leq 20$ K. For the sample with $x=0.9$, the fit yields $B=6.1$ mJ/mol K² and $T_0=4.5$ K for temperatures in the range $1 \text{ K} \leq T \leq 6$ K. The $\Delta C(T)$ data have also been fitted by a power law, which is predicted by several NFL models, including the Griffith's phase model.²⁰ The power-law fits are shown as dashed lines in Fig. 10. The data for the sample with $x=0.8$ cannot be described by a power law over any significant temperature range. The data for the sample with $x=0.9$ are consistent with a power law for temperatures in the range $1 \leq T \leq 6$ K. We have also attempted to fit the data with the form $\Delta C(T)/T = \gamma_0 + B'T^{1/2}$, which is predicted for NFL systems in the vicinity of a quantum critical point at which a spin-glass freezing temperature has been suppressed to $T=0$ K.^{16,18} These fits are shown as dotted lines in Fig. 10, and do not describe our data for either sample over any appreciable temperature range.

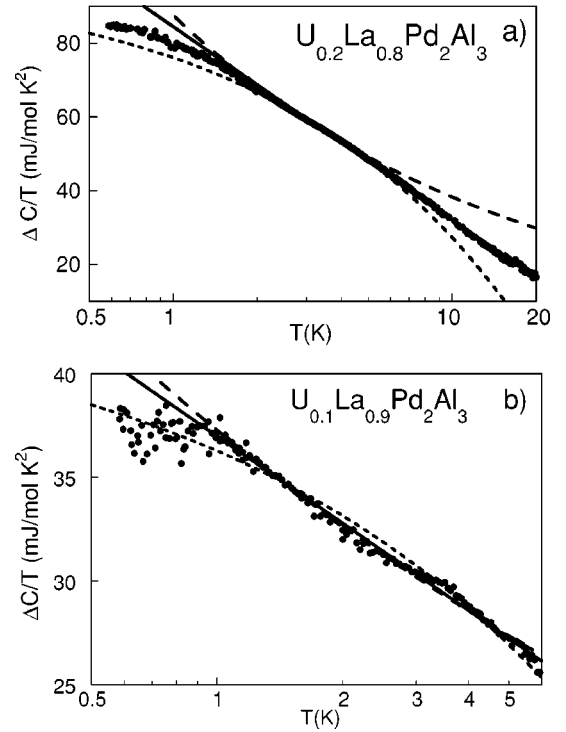


FIG. 10. Specific heat ΔC divided by temperature T vs T on a log scale for the samples with $x=0.8$ (a) and $x=0.9$ (b). The specific heat of the LaPd_2Al_3 end member has been subtracted from each data set to remove the phonon contribution. The solid circles represent the data, and the solid straight lines are fits of $\Delta C(T)/T = -B \ln(T/T_0)$ to the $\Delta C(T)/T$ data, where B and T_0 are adjustable parameters. The dashed lines are fits of a power-law T dependence $\Delta C(T)/T \propto T^m$, and the dotted lines are fits of $\Delta C(T)/T = \gamma_0 + B'T^{1/2}$ to the $\Delta C(T)/T$ data.

The LaPd_2Al_3 compound shows features in $\rho(T)$ and $C(T)$ indicative of superconductivity. As shown in Fig. 11, $\rho(T)$ drops sharply to zero between $T=0.9$ K and $T=0.8$ K, and $C(T)/T$ shows a jump at $T=0.8$ K. We calcu-

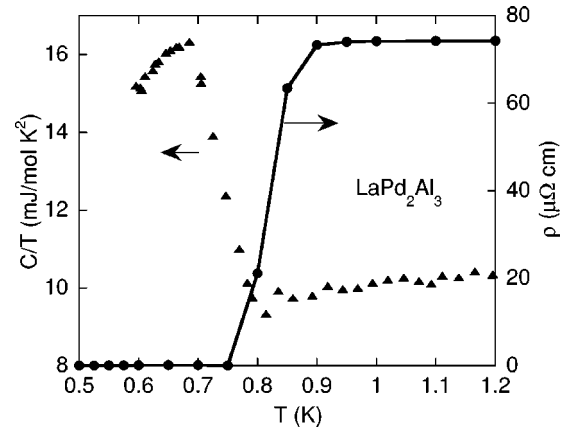


FIG. 11. Resistivity ρ (circles) and specific heat C divided by temperature T (triangles) as a function of T for LaPd_2Al_3 . The jumps in $\rho(T)$ and $C(T)/T$ indicate a superconducting transition. The midpoint of this transition in $\rho(T)$ occurs at $T_c=0.85$ K. The superconducting transition determined from an equal entropy construction of $C(T)/T$ occurs at $T_c=0.74$ K.

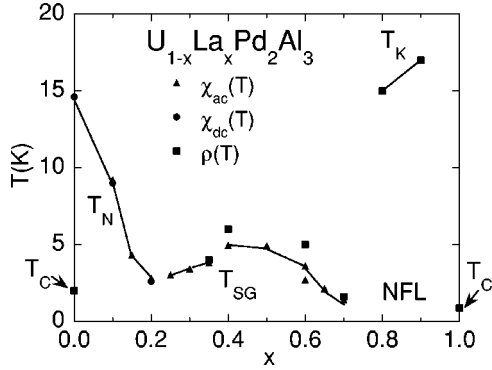


FIG. 12. The Néel temperature T_N , spin-glass freezing temperature T_{SG} , superconducting transition temperature T_C , and Kondo temperature T_K plotted as a function of lanthanum concentration x for the $U_{1-x}La_xPd_2Al_3$ system. T_N and T_{SG} are determined from kinks in the dc susceptibility χ_{dc} (circles), peaks in the ac susceptibility χ_{ac} (triangles) and kinks in the resistivity $\rho(T)$ (squares). The superconducting transitions are determined from the 50% point of the resistivity transitions. T_K is the Kondo temperature determined from high-temperature resistivity data for the samples with $x=0.8$ and 0.9 . NFL temperature dependences of the resistivity and specific heat are observed at low temperatures for the samples with $x=0.8$ and 0.9 .

lated $\Delta C/\gamma T_c=0.8$, which suggests that the superconductivity in this compound is a bulk phenomenon. A value for the bulk T_c of 0.74 K was derived from an equal entropy construction of the $C(T)$ data.

The phase diagram of the $U_{1-x}La_xPd_2Al_3$ system is shown in Fig. 12. The temperatures of the kinks in $\chi_{dc}(T)$, the peaks in $\chi_{ac}(T)$, and the peaks in $\rho(T)$ are plotted as a function of x . The samples with $0 \leq x \leq 0.2$ exhibit long-range magnetic order whereas the samples with $0.25 \leq x \leq 0.65$ form a spin glass at low temperatures. The samples that exhibit spin-glass behavior with $0.25 \leq x \leq 0.35$ show a scaling of T_{SG} and χ_{ac} with x . Although peaks in $\rho(T)$ are not usually associated with spin-glass freezing, we have included them in the phase diagram since they track T_{SG} as determined from the $\chi_{ac}(T)$ data.

IV. DISCUSSION

A. Magnetic behavior

The presence of magnetic relaxation and frequency-dependent peaks in $\chi_{ac}(T)$ for the samples with $0.25 \leq x \leq 0.65$ indicates that these samples exhibit spin-glass freezing at low temperatures. It is not unexpected that a spin glass would form in this system since the presence of magnetic uranium and nonmagnetic lanthanum on the same lattice site produces disorder. Spin-glass behavior has also been seen in the $U_{1-x}Y_xPd_2Al_3$ system for $0.3 \leq x \leq 0.6$.²⁸ The $\chi_{ac}(T)$ data for the samples with $x=0.4, 0.5$, and 0.6 have a double-peak feature that could be due to the presence of two slightly different concentrations of lanthanum. This kind of impurity would result in a slight broadening of the x-ray-diffraction peaks, and would be extremely difficult to detect.

The samples with $x < 0.2$ show no indications of spin-glass behavior, therefore, it is reasonable to assume that the

peaks in $\chi_{ac}(T)$ and kinks in $\chi_{dc}(T)$ are due to the onset of antiferromagnetic ordering. The Néel temperature is suppressed from $T_N=14.6$ K for the parent compound UPd_2Al_3 to $T_N=2.6$ K for the sample with $x=0.2$.

Fits of the dc magnetization to a Curie-Weiss law for the samples with $0.1 \leq x \leq 0.8$ result in values of μ_{eff} , which are suppressed from the free uranium ion moment of $3.56\mu_B$. Based on x-ray photoemission spectroscopy (XPS) measurements on UPd_2Al_3 , Fujimori *et al.* have suggested that the uranium ion exhibits intermediate valence between the 3+ and 4+ states, which could account for the low value of μ_{eff} .³³ Since there is significant Kondo scattering in this system, it is also likely that Kondo screening of the the uranium 5f moments by conduction electrons is suppressing μ_{eff} . The highest effective moments were found for samples exhibiting spin-glass behavior, the significance of which is unclear.

Our data generally agree with the results of Sakon *et al.* for the same system.³⁰ Sakon *et al.* observed pronounced Kondo scattering in $\rho(T)$ manifested as $d\rho/dT < 0$ for the samples with $x=0.5$ and 0.75 . Based on anomalies in $\chi(T)$, Sakon *et al.* obtained Néel temperatures of 9 and 3 K for the samples with $x=0.1$ and 0.25 , respectively. This is in accordance with our data, although we attribute the transition for the $x=0.25$ sample to spin-glass freezing, rather than long-range order. For the sample with $x=0.5$, Sakon *et al.* found hysteresis in the magnetization that they attributed to ferromagnetism. They also saw a broad bump in $C(T)$ around $T=5$ K. Our results from magnetic relaxation and frequency dependence of $\chi_{ac}(T)$ indicate that the transition at $T \sim 5$ K is a spin-glass freezing transition rather than a transition to ferromagnetic order.

It is interesting to compare the effect of lanthanum substitution in UPd_2Al_3 with the substitution of other atoms. Detailed studies of the magnetic phase diagrams have been performed on two other systems, $U_{1-x}Y_xPd_2Al_3$ and $U_{1-x}Th_xPd_2Al_3$.^{23,28,32} The phase diagrams of $U_{1-x}La_xPd_2Al_3$ and $U_{1-x}Y_xPd_2Al_3$ are remarkably similar. Both show a region of AFM order, followed by spin-glass freezing that is suppressed to zero temperature. By contrast, the $U_{1-x}Th_xPd_2Al_3$ system shows very little suppression of T_N with increasing x , and shows no indication of spin-glass freezing. Since both yttrium and lanthanum are trivalent, whereas thorium is tetravalent, it seems that the magnetic behavior in these systems is primarily determined by the valence of the substituent element.

B. NFL behavior

The NFL temperature dependences of $\rho(T)$ and $C(T)/T$ for the $U_{1-x}La_xPd_2Al_3$ system in the NFL regime have the following forms:

$$\rho(T)/\rho(0) = 1 - AT^n, \quad n = 1.3 \quad (1)$$

$$C(T)/T = -B \ln(T/T_0) \quad (2)$$

These forms are similar to those found in other f -electron systems which exhibit NFL behavior including $U_{1-x}Th_xPd_2Al_3$ with $0.6 \leq x \leq 0.99$, and $Y_{1-x}U_xPd_3$ with $0.1 \leq x \leq 0.2$.^{6,22,34} In particular, the logarithmic dependence of $C(T)/T$ at low temperatures seems to be a universal feature of f -electron NFL systems.

The temperature dependences of $\rho(T)$ in the NFL regime are very similar for the $U_{1-x}Th_xPd_2Al_3$ and $U_{1-x}La_xPd_2Al_3$ systems, but dramatically different for the $U_{1-x}Y_xPd_2Al_3$ system. Both $U_{1-x}Th_xPd_2Al_3$ and $U_{1-x}La_xPd_2Al_3$ show a Kondo effect with $d\rho/dT < 0$ at the lowest temperatures, and power-law behavior of $\rho(T)$ with an exponent $n \sim 1.3-1.5$. In contrast, $\rho(T)$ in the $U_{1-x}Y_xPd_2Al_3$ system decreases linearly with decreasing temperature in the NFL regime. Thus, it seems that in these systems the valence of the substituent element is not driving the behavior of $\rho(T)$ in the NFL regime. If the valence were important, we would expect that substitution of trivalent lanthanum and yttrium would yield similar forms for $\rho(T)$, whereas substitution of tetravalent thorium would result in different behavior. One attribute that lanthanum and thorium do have in common is similar atomic radii that are larger than the atomic radius of uranium. The x-ray-diffraction data show that substitution of thorium or lanthanum causes the lattice of UPd_2Al_3 to expand, whereas substitution of yttrium does not cause a detectable change in the lattice parameters a or c . Perhaps the increase in the interionic spacing in the $U_{1-x}La_xPd_2Al_3$ and $U_{1-x}Th_xPd_2Al_3$ systems causes single-ion effects to become more important in the NFL regime than in the $U_{1-x}Y_xPd_2Al_3$ system in which the uranium ions are more dense.

There is no theory to date that predicts the behavior observed for both $\rho(T)$ and $C(T)/T$ of the $U_{1-x}La_xPd_2Al_3$ system in the NFL regime. Since the NFL behavior occurs in the dilute magnetic limit, it seems reasonable that the NFL behavior could result from single-impurity effects. Currently, the only single-impurity model for NFL behavior is the two-channel spin-1/2 quadrupolar Kondo model. In this theory, the electronic specific heat is predicted to be

$$C(T)/T = -bR/T_K \ln(T/b'T_K), \quad (3)$$

where b has been calculated to be about 0.25, R is the ideal gas constant, T_K is the Kondo temperature, and $b' \sim 0.41$.^{11,35} This prediction for the specific heat is consistent with our measurements for $U_{1-x}La_xPd_2Al_3$. However, the prediction for the resistivity in the two-channel spin-1/2 Kondo effect is

$$\rho(T)/\rho(0) = 1 - a(T/T_K), \quad 0.05T_K < T < T_K \quad (4)$$

$$\rho(T)/\rho(0) = 1 - a(T/T_K)^{1/2}, \quad T < 0.05T_K \quad (5)$$

which is inconsistent with our results. For the $U_{1-x}La_xPd_2Al_3$ samples with $x=0.8$ and 0.9 , $\rho(T)$ follows a power law with $n=1.3$, and this power-law behavior extends down to the lowest temperatures measured ($0.005T_K$) for the sample with $x=0.9$.

Although the temperature dependence of $\rho(T)$ in the $U_{1-x}La_xPd_2Al_3$ system is not consistent with the two-channel spin-half Kondo model, it is still possible that the

TABLE II. Kondo temperatures for samples of $U_{1-x}La_xPd_2Al_3$ with $x=0.8$ and 0.9 determined from measurements of specific heat (T_{K-C}), magnetic susceptibility ($T_{K-\chi}$), electrical resistivity at high temperatures ($T_{K-\rho H}$), and at low temperatures ($T_{K-\rho L}$).

x	T_{K-C} (K)	$T_{K-\chi}$ (K)	$T_{K-\rho H}$ (K)	$T_{K-\rho L}$ (L)
0.8	18	10	15	16
0.9	34	30	17	18

behavior in this system is driven by single-ion effects. If single-ion Kondo physics dominates the $U_{1-x}La_xPd_2Al_3$ system, then a single energy scale, given by the Kondo temperature, should characterize the behavior of the physical properties at all temperatures. Thus, the values of T_K that are extracted from the $C(T)$, $\chi(T)$, and $\rho(T)$ data should be consistent with each other. It was shown in Fig. 8 that the high-temperature resistivity yields $T_K=15$ and 17 K for the samples with $x=0.8$ and 0.9 , respectively. We will refer to this Kondo temperatures as $T_{K-\rho H}$. The Kondo temperature can also be estimated from the slope of C/T vs $\ln T$ using the prediction of the quadrupolar Kondo model (3). Using the result³⁵ that $b \sim 0.25$, we find that $T_{K-C} = 18$ K for the sample with $x=0.8$ and $T_{K-C} = 34$ K for the sample with $x=0.9$. T_K can also be estimated from the magnetic susceptibility. For the Kondo model, $T_{K-\chi} = -\theta_{CW}/d$, where d is 3 or 4. Taking $d=3$, this yields $T_{K-\chi} = 10$ K for $x=0.8$ and $T_{K-\chi} = 30$ K for $x=0.9$. The low-temperature resistivity can be expressed as

$$\rho(T)/\rho(0) = 1 - a(T/T_K)^{1.3}, \quad (6)$$

where a is an undefined phenomenological parameter, similar to the analysis performed for the $U_{1-x}Th_xPd_2Al_3$ and the $Y_{1-x}U_xPd_3$ systems.^{22,34} In the $Y_{1-x}U_xPd_3$ system, a was determined to be 0.23 using the Kondo temperature derived from specific-heat measurements, and in the $U_{1-x}Th_xPd_2Al_3$ system, a was determined to be 0.3 using the Kondo temperature inferred from high-temperature resistivity measurements. If we choose the value of $a=0.3$ obtained for the $U_{1-x}Th_xPd_2Al_3$ system, we find $T_{K-\rho L} = 16$ K for the sample with $x=0.8$ and $T_{K-\rho L} = 18$ K for the sample with $x=0.9$.

The estimates of T_K from the various physical properties of the $U_{1-x}La_xPd_2Al_3$ system are in rough agreement, ranging from 10 to 18 K for the sample with $x=0.8$, and 17–34 K for the sample with $x=0.9$. The Kondo temperatures are summarized in Table II. The values are remarkably close given that T_K is a characteristic energy scale, not a precise transition temperature. Thus, based on the analysis of the Kondo temperatures from the various physical properties of the $U_{1-x}La_xPd_2Al_3$ system, the data are consistent with a single-ion Kondo model. A further test of the single-ion model for $U_{1-x}La_xPd_2Al_3$ would be to see if $\rho(T)$, $C(T)/T$, and $\chi(T)$ scale with x in the NFL regime. A similar analysis has been performed for $U_{1-x}Th_xPd_2Al_3$ in which it was determined that ρ_0 scales with uranium concentration for $0.6 \leq x \leq 0.99$, and that a single energy scale dominates the behavior in the NFL regime.²²

There are a number of theories that postulate that NFL behavior is driven by collective effects, rather than single-ion

effects in the vicinity of a $T=0$ K quantum critical point. In 1995, two groups investigated a model in which a spin-glass freezing temperature T_{SG} is suppressed to $T=0$ K giving rise to unusual scaling behaviors in the various physical quantities.^{17,18} Since the NFL behavior in the $U_{1-x}La_xPd_2Al_3$ system occurs near the lanthanum concentration, where the spin-glass freezing temperature drops below the low-temperature limit of the experiments, this model could be applicable. Sengupta and Georges predicted¹⁸ that the electrical resistivity should follow the relation $\rho(T) \sim T^{3/2}$. This is close to the power-law exponent $n=1.3$, which we found for the samples with $x=0.8$ and 0.9 . However, they also predict that the specific heat divided by temperature $C(T)/T$ should follow a $T^{1/2}$ temperature dependence, which is inconsistent with our results.

The alloyed nature of the $U_{1-x}La_xPd_2Al_3$ compounds and the presence of spin-glass freezing in a portion of the phase diagram suggests that disorder could be a significant factor in determining the NFL behavior. There are two NFL models to date that incorporate the effects of disorder: the Kondo disorder model¹⁹ and the Griffith's phase model.²⁰ The Kondo disorder model predicts a logarithmic dependence of $C(T)/T$, which describes our results for the samples of $U_{1-x}La_xPd_2Al_3$ with $x=0.8$ and 0.9 . However, the resistivity was shown to follow a linear dependence, which is inconsistent with our results. The Griffith's phase model predicts a power-law dependence in the specific heat, which is consistent with the data for the sample with $x=0.9$, but not the sample with $x=0.8$. No prediction for the resistivity has emerged from the Griffith's phase model, so we cannot draw a definite conclusion as to whether this model describes the NFL behavior in the $U_{1-x}La_xPd_2Al_3$ system.

V. SUMMARY

We have performed measurements of the specific heat, electrical resistivity, and magnetic susceptibility as a function of temperature for polycrystalline samples of $U_{1-x}La_xPd_2Al_3$. The Néel temperature T_N is sharply suppressed with increasing lanthanum concentration, dropping from $T_N=14.6$ K at $x=0$ to $T_N=2.6$ K at $x=0.2$. For lanthanum concentrations in the region $0.25 \leq x \leq 0.65$, spin-glass freezing is observed in χ_{ac} and χ_{dc} with freezing temperatures T_{SG} between $T=2$ and 5 K. The samples with $0.25 \leq x \leq 0.35$ exhibit a linear dependence of the spin-glass freezing temperature and the peak value of $\chi_{ac}(T)$ with x . The spin-glass freezing temperature extrapolates to $T=0$ K near $x=0.8$. The samples with $x=0.8$ and 0.9 exhibit NFL behavior in the electrical resistivity and specific heat. The resistivity at low temperatures can be described by a power-law temperature dependence with an exponent $n=1.3 \pm 0.1$ for $T < 10$ K. The specific heat is consistent with the relation

$$C/T = -B \ln(T/T_0) \quad (7)$$

for the samples with $x=0.8$ and 0.9 . This behavior persists for temperatures in the range $3 \leq T \leq 20$ K for the sample with $x=0.8$, and $1 \leq T \leq 6$ K for the sample with $x=0.9$. There is no theoretical model to date that predicts the temperature dependences of both $C(T)$ and $\rho(T)$ in the NFL regime.

ACKNOWLEDGMENTS

This work was supported by the U.S. Department of Energy under Grant No. DE FG03-86ER-45230 and by the National Science Foundation under Grant No. DMR-00-72125.

-
- ¹S. R. Julian, C. Pfleiderer, F. M. Grosche, N. D. Mathur, G. J. McMullan, A. J. Diver, I. R. Walker, and G. G. Lonzarich, *J. Phys.: Condens. Matter* **8**, 9675 (1996).
- ²F. Steglich, B. Buschinger, P. Gegenwart, M. Lohmann, R. Hellrich, C. Langhammer, P. Hellmann, L. Donnevert, S. Thomas, A. Link, C. Geibel, M. Lang, G. Sparn, and W. Assmus, *J. Phys.: Condens. Matter* **8**, 9909 (1996).
- ³F. Steglich, P. Gegenwart, C. Geibel, P. Hinze, M. Lang, C. Langhammer, G. Sparn, and O. Trovarelli, *Physica B* **280**, 349 (2000).
- ⁴I. R. Walker, F. M. Grosche, D. M. Freye, and G. G. Lonzarich, *Physica C* **282–287**, 303 (1997).
- ⁵F. M. Grosche, S. R. Julian, N. D. Mathur, and G. G. Lonzarich, *Physica B* **223&224**, 50 (1996).
- ⁶M. B. Maple, M. C. de Andrade, J. Herrmann, Y. Dalichaouch, D. A. Gajewski, C. L. Seaman, R. Chau, R. Movshovich, M. C. Aronson, and R. Osborn, *J. Low Temp. Phys.* **99**, 223 (1995).
- ⁷B. Andraka and G. R. Stewart, *Phys. Rev. B* **47**, 3208 (1993).
- ⁸R. Chau and M. B. Maple, *J. Phys.: Condens. Matter* **8**, 9939 (1996).
- ⁹P. Nozières and A. Blandin, *J. Phys. (Paris)* **41**, 193 (1980).
- ¹⁰I. Affleck and A. W. W. Ludwig, *Nucl. Phys. B* **360**, 641 (1991).
- ¹¹P. D. Sacramento and P. Schlottmann, *Phys. Rev. B* **43**, 13 294 (1991).
- ¹²D. L. Cox, *Phys. Rev. Lett.* **59**, 1240 (1987).
- ¹³J. A. Hertz, *Phys. Rev. B* **14**, 1165 (1976).
- ¹⁴A. J. Millis, *Phys. Rev. B* **48**, 7183 (1993).
- ¹⁵A. M. Tselvelik and M. Reizer, *Phys. Rev. B* **48**, 9887 (1993).
- ¹⁶S. Sachdev and J. Ye, *Phys. Rev. Lett.* **69**, 2411 (1992).
- ¹⁷S. Sachdev, N. Read, and R. Oppermann, *Phys. Rev. B* **52**, 10 286 (1995).
- ¹⁸A. M. Sengupta and A. Georges, *Phys. Rev. B* **52**, 10 295 (1995).
- ¹⁹E. Miranda, V. Dobrosavljevic, and G. Kotliar, *J. Phys.: Condens. Matter* **8**, 9871 (1996).
- ²⁰A. H. Castro Neto, G. Castilla, and B. A. Jones, *Phys. Rev. Lett.* **81**, 3531 (1998).
- ²¹M. B. Maple, C. L. Seaman, D. A. Gajewski, Y. Dalichaouch, V. B. Barbetta, M. C. de Andrade, H. A. Mook, H. G. Lukefahr, O. O. Bernal, and D. E. MacLaughlin, *J. Low Temp. Phys.* **95**, 225 (1994).
- ²²R. P. Dickey, A. Amann, E. J. Freeman, M. C. de Andrade, and M. B. Maple, *Phys. Rev. B* **62**, 3979 (2000).
- ²³E. J. Freeman, M. C. de Andrade, R. P. Dickey, N. R. Dilley, and M. B. Maple, *Phys. Rev. B* **58**, 16 027 (1998).

- ²⁴C. Geibel, C. Schank, S. Thies, H. Kitazawa, C. D. Bredl, A. Bohm, M. Rau, A. Grauel, R. Caspary, R. Helfrich, U. Ahlheim, G. Weber, and F. Steglich, *Z. Phys. B: Condens. Matter* **84**, 1 (1991).
- ²⁵C. Geibel, C. Schank, F. Jährling, B. Buschinger, A. Grauel, T. Lühmann, P. Gegenwart, R. Helfrich, P. H. P. Reinders, and F. Steglich, *Physica B* **199&200**, 128 (1994).
- ²⁶A. Grauel, A. Böhm, H. Fischer, C. Geibel, R. Köhler, R. Modler, C. Schank, F. Steglich, G. Weber, T. Komatsubara, and N. Sato, *Phys. Rev. B* **46**, 5818 (1992).
- ²⁷D. A. Gajewski, N. R. Dilley, R. Chau, and M. B. Maple, *J. Phys.: Condens. Matter* **8**, 9793 (1996).
- ²⁸R. P. Dickey, E. J. Freeman, V. S. Zapf, P.-C. Ho, and M. B. Maple (unpublished).
- ²⁹M. B. Maple, A. Amann, R. P. Dickey, E. J. Freeman, C. Sirvent, M. C. de Andrade, and N. R. Dilley, *Physica B* **281&282**, 332 (2000).
- ³⁰T. Sakon, K. Imamura, N. Koga, N. Sato, and T. Komatsubara, *Physica B* **206&207**, 427 (1995).
- ³¹R. Tournier and Y. Ishikawa, *Phys. Lett.* **11**, 280 (1964).
- ³²Y. Dalichaouch and M. B. Maple, *Physica B* **199&200**, 176 (1994).
- ³³S. Fujimori, Y. Saito, N. Sato, T. Komatsubara, S. Suzuki, S. Sato, and T. Ishii, *Solid State Commun.* **105**, 185 (1997).
- ³⁴M. B. Maple, R. P. Dickey, J. Herrmann, M. C. de Andrade, E. J. Freeman, D. A. Gajewski, and R. Chau, *J. Phys.: Condens. Matter* **8**, 9773 (1996).
- ³⁵P. D. Sacramento and P. Schlottmann, *Phys. Lett. A* **142**, 245 (1989).